Carbon-Sandwiched Perovskite Solar Cell

Namyoung Ahn[1†], Il Jeon[2†], Jungjin Yoon[1], Esko I. Kauppinen[3], Yutaka Matsuo[2]*, Shigeo Maruyama[2]*, Mansoo Choi[1]*

[1]Department of Mechanical and Aerospace Engineering, Seoul National University, Seoul 08826, Korea.
E-mail: mchoi@snu.ac.kr
I. Jeon, Prof. Y. Matsuo, Prof. S. Maruyama
[2]Department of Mechanical Engineering, The University of Tokyo, Tokyo 113- 8656, Japan
E-mail: matsuo@photon.t.u-tokyo.ac.jp, maruyama@photon.t.u-tokyo.ac.jp
E. I. Kauppinen
[3]Department of Applied Physics, Aalto University School of Science, FI-00076 Aalto, Finland

† These authors contributed equally to this work

* Corresponding authors

E-mail: mchoi@snu.ac.kr, matsuo@photon.t.u-tokyo.ac.jp, maruyama@photon.t.u-tokyo.ac.jp

Abstract

Promising perovskite solar cell technology with soaring power conversion efficiencies share common problems of low stability and high cost. This work provides the solution to these problems by employing carbon sandwich structure, in which fullerene bottom layer resolves the stability issue and carbon nanotube top electrode layer offers high stability and low-cost merits. Devices fabricated using different hole-transporting materials infiltrated into carbon nanotube networks were examined for performance and stability under constant illumination in air. Polymeric hole-transporting layers show much higher stability when combined with the carbon nanotubes, due to their compact nature and stronger interaction with the carbon network. As the result, the encapsulated device shows high stability against both air and light, with around 90% of the initial efficiency after 2000 hours under actual operation conditions. Cost analysis also shows that using the polymeric hole-transporting materials in carbon nanotube films brings the fabrication cost down to less than 5.5% compared with conventional devices.

Our finding will pave the way toward highly stable and low-cost perovskite photovoltaic technologies for the coming future.

Introduction

Since Miyasaka and colleagues adopted perovskite semiconductors into photovoltaic devices,[1] and Park and colleagues realized solidified lead halide perovskite,[2] perovskite solar cells (PSCs) have received much attention on account of high power conversion efficiency (PCE) and other advantages of organic solar cells.[3–5] Their reported PCEs have soared rapidly in the last five years, and now some certified efficiencies exceed 20%.[6,7] However, there remains critical shortcomings, prominently high-cost and stability[8] that need to be addressed. Numerous research groups around the world are working on these issues. To reduce the fabrication cost, hole-conductor and metal-free PSCs have been suggested,[9–11] and more stable materials with more encapsulating structures are under intense research.[12–14] As a solution to the aforementioned drawbacks, carbon nanotube (CNT) film has shown to be effective in replacing metal electrodes and enhancing the stability of PSCs in air. For example, Snaith and colleagues[15] and Matsuda and colleagues[16] have demonstrated that hydrophobic nature of CNTs can function as an effective passivation. Nevertheless, they relied on expensive gold electrodes[9]. Li et al.,[17] and Aitola et al.,[18] used aerosol-produced single-walled CNTs as top electrodes to replace metals and hole-conductors and high temperature-annealed TiO_2, which translate to relatively low performance and high hysteresis, respectively.[19] The use of C_{60} as an electron transport layer has been reported to be a better alternative.[20–22]

Here, we report PSCs in which lead halide perovskite layer is sandwiched by C_{60} and single-walled CNTs (SWCNTs) without metal electrodes. Such carbon allotropes-sandwich approach led to low-cost fabrication by removing expensive metal electrodes, furthermore, enabled room

temperature process and assured long-term stability by preventing moisture penetration and charge trapping[23] via highly effective electron extracting layer of C_{60} and hydrophobic SWCNT electrodes. The air-processed PSCs with a configuration of indium tin oxide (ITO)/C_{60}/$CH_3NH_3PbI_3$/CNT were tested for the perspectives of stability and cost by infiltrating three mainstream hole-transporting materials (HTMs), namely, 2,2',7,7'-tetrakis(N,N-di-p-methoxyphenylamino)-9,9'-spirobifluorene (spiro-MeOTAD)[2,24–26], poly[bis(4-phenyl)(2,4,6-trimethylphenyl)amine] (PTAA)[27], and poly(3-hexylthiophene-2,5-diyl) (P3HT) into porous SWCNT electrode.[28,29]

Results and discussion

First, the carbon-sandwiched perovskite device without a HTM was studied by using aerosol-synthesized CNT[30,31] on top of $MAPbI_3$ (ITO/C_{60}/$MAPbI_3$/CNT). To confirm stability and hysteresis improvement via carbon-sandwiched approach by harnessing C_{60}, we compared two types of devices with structural configurations: ITO/C_{60}/$MAPbI_3$/CNT (**Fig. 1a**) and FTO/TiO_2/$MAPbI_3$/CNT (**Fig. 1b**). Photovoltaic characteristics and *J-V* curves of two devices can be seen in **Table 1**. The C_{60}-based device show higher photovoltaic performance than the TiO_2-based device. Moreover, there is a dramatic improvement in terms of J-V curve hysteresis for the C60-based device. As shown in **Fig. 1c and 1d**, their forward and backward scan of $J-V$ curves show that the C_{60}-based devices show negligible photocurrent hysteresis, while TiO_2-based devices show severe photocurrent hysteresis. Considering that such photocurrent hysteresis is induced by charge trapping, the device with severe hysteresis can be deteriorated by trapped-charge driven degradation of perovskite materials[23]. To confirm the effect of charge trapping on device stability, we measured normalized PCEs as a function of time measured under a constant illumination of one sun in ambience without encapsulation as can be seen in **Fig. 1g**. It is notable that normalized PCEs of the TiO_2-based devices decayed faster

than those of the C_{60}-based device over time under the same condition. These observations are likely to be indicative of a strong correlation between hysteresis and device stability.

ITO/C_{60}/$MAPbI_3$/CNT devices without additional HTM gave an efficiency of 13.2% and showed high reproducibility with an average PCE of 12.4 ± 0.9% (**Table 2**). However, additional HTM infiltration into the porous SWCNTs could enhance performance and stability. To examine the effect of additional HTMs, we employed three HTMs: spiro-MeOTAD, PTAA, and P3HT. The cross-sectional scanning electron microscopy (SEM) images show that HTMs were thoroughly infiltrated inside the CNT network (**Fig. S1**). Addition of spiro-MeOTAD, PTAA, and P3HT increased the PCE to 17.0%, 15.3%, and 13.6%, respectively (**Fig. 2a and b, Table 1**). Upon the addition of HTM, the improvement in PCEs resulted from the increases in J_{SC} and V_{OC} due to better energy alignment and increased carrier density, and higher fill factor (FF) due to improved hole-transporting ability. All HTM-added devices showed negligible hysteresis as expected (**Table S1**). The addition of HTMs brings us another effect in terms of protecting the infiltration of water vapor, which results in improved device stability. When the devices were tested under one sun illumination in atmosphere, the HTM-applied devices showed much higher stability than the CNT-only devices without additional HTM (**Fig. 2c**). This means that the hydrophobic CNT film alone was not enough to block out the atmospheric moisture and that application of HTM is crucial in obtaining long-term stability. Addition of the HTM not only reinforced the hole-transporting ability of CNT, but also functioned as an encapsulation by filling up the CNT network.[32,33] The HTM-applied devices showed even higher stability than the reference devices using gold. This clearly serves as a gauge that CNT-laminated devices show excellent stability. Among the different HTMs, the devices with P3HT and PTAA exhibited much higher stability than those with spiro-MeOTAD. To investigate the reason, we did water vapor transmittance rate (WVTR) measurement to find

out shows the moisture barrier ability of the CNT and HTM-added CNT films (**Fig. 2d and Fig. S2**). Even though Snaith and his colleagues compared the thermal stability of those three HTMs briefly, there has not been a detailed account on the moisture passivation mechanism.[17] As shown in **Fig. 2d**, a CNT film without a HTM showed a large value of WVTR agreeing with its poor water barrier ability and significantly low stability shown in **Fig. 2c**.

The HTM-added CNT films showed much higher barrier ability than the case without HTM and their WVTR trend matched the stability trend among the HTMs (See **Fig. 2c and 2d**). Such different barrier ability could be inferred from different molecular structure. Comparing the three HTMs, chain-like polymers (PTAA and P3HT) can seal CNTs more effectively than unchained spiro-MeOTAD. Moreover, the conjugated polymers can induce π–π interaction with CNTs, forming supramolecular CNT-polymer hybrids explaining their lower WVTR values.[33–35] We also did computational calculations of P3HT and PTAA to investigate their molecular configurations.[36] As shown in **Fig. 3a and Fig. S3**, P3HT has a planar configuration while PTAA has a staggered configuration due to the steric effect. Planar P3HT's conformation allows stacked crystallization leading to a more closely packed structure, which results in P3HT being more water-tight than PTAA when they aggregate (**Fig. 3b**). P3HT forming a densely-packed crystallite was previously confirmed experimentally using x-ray diffraction (XRD) from literatures.[37,38] Moreover, planar P3HT has been reported to closely interact with CNT by wrapping around nanotubes, indicating a good integration with CNT using π-π interaction (**Fig. 3c**).[39,40] However, PTAA having staggered conformation could not stick to the nanotubes. Thus, P3HT forms a more effective nanohybrid with the CNTs than PTAA. While *p*-doping lithium salt is commonly added to increase hole mobility[41–44], the stability of PSCs could be lowered due to its hygroscopic nature. In addition, the dopant-added P3HT CNT film showed an increase in water permeability. (**Fig. 2d** (WVTR data)) Thus, we conclude that P3HT, which

functions as a HTM without the need for ionic dopants, would be the best choice for the solution to achieve high stability and low cost for PSCs.[28]

To date, many cases of reported PSCs claiming high stability have been tested with using a UV-filter, or under low light intensity, sometimes in dark condition, or in nitrogen-filled glovebox [45-50]. However, the proper stability test of PSCs should be carried out under light illumination in real atmosphere to confirm the possibility of their practical use. Therefore, we monitored the *J-V* characteristics of best-performing ITO/C_{60}/$MAPbI_3$/P3HT/CNT devices with glass encapsulation under AM 1.5G one sun illumination including UV radiation in ambient air up to 2200 hours (see **Fig. 3d-f**). We used a conventional encapsulation with glass cover using UV curing resin without any special technique [47]. Our encapsulated device maintained up to 85 % of its initial PCE after 2200 hours, demonstrating the state-of-the-art long-term operational stability among literatures.

Another merit of our carbon-sandwiched PSCs should be low fabrication cost, which is mainly attributed to the replacement of expensive metal electrodes such as gold with CNT films. Even if we consider relatively cheaper metals, for example silver and aluminium, there are some limitations for PSC commercialization due to their cost and reactivity to iodine of perovskite and oxygen in air[51]. Also, Spiro-MeOTAD is known to be expensive compared to other raw materials used in PSCs because it should be prepared through a difficult and costly synthetic route. [9,52] Accordingly, our carbon-sandwiched approach (ITO/C_{60}/$MAPbI_3$/P3HT/CNT) brings down the cost greatly due to earth-abundant nature of carbon materials and air stability. To confirm the cost-effectiveness, we conducted the cost analysis in lab-scale fabrication as shown in **Table S2** and **Fig. S4**. Our devices bring down the fabrication cost to less than 5.5% compared to that of conventional devices (fluorine-doped tin oxide (FTO)/TiO_2/mesoporous-

TiO_2/$MAPbI_3$/spiro-MeOTAD/Au). If we take into account fabrication set-up, production time in a mass scale, the cost can be expected to go down even further because of low-temperature processability.

Conclusion

In conclusion, air-processed PSCs with a configuration of ITO/C_{60}/$MAPbI_3$/CNT without a HTM produced a PCE of 13.2% with a cost-down to less than 5.5% compared to that of the conventional devices. Upon the addition of a HTM onto CNT, it significantly enhanced PCE and stability. Addition of spiro-MeOTAD increased PCE to 17%, which is the record-high efficiency among the CNT-laminated solar cells. Nevertheless, we think the fabrication cost is relatively high and the stability should be improved higher. Application of the polymeric HTMs improved the stability even further at the expense of PCE. In this regard, the application of P3HT demonstrated much better stability than PTAA due to its more compact packing and enhanced interaction with CNTs. Simple glass encapsulation of our carbon-sandwiched ITO/C_{60}/$MAPbI_3$/P3HT/CNT devices demonstrated unsubsided stability up to 2200 hours under constant illumination of one sun (100% light intensity),without UV-filter, in ambient conditions. The development of more sophisticated encapsulation techniques should improve further the stability of our carbon-sandwiched PSCs.

Experimental Section

Synthesis of CNT Films. Randomly oriented CNT networks with high purity and long nanotube bundle length can be synthesized by the aerosol chemical vapour deposition (CVD) method[33,34]. The floating catalyst aerosol CVD was carried out in a scaled-up reaction tube with a diameter of 150 mm. The catalyst precursor was vaporised by passing ambient temperature CO through a cartridge filled with ferrocene powder. To obtain stable growth of

CNTs, a controlled amount of CO_2 was added with the carbon source (CO). CNTs were directly collected downstream of the reactor by filtering the flow through a nitrocellulose or silver membrane filter (Millipore Corp., USA; HAWP, 0.45 μm pore diameter). The flow containing ferrocene vapour was then introduced into the high-temperature zone of a ceramic tube reactor through a water-cooled probe and mixed with additional CO. Ferrocene vapour was thermally decomposed in the gas phase of the aerosol CVD reactor at the 880 ˚C. The CO gas was supplied at 4 L min^{-1} and decomposed on the iron nanoparticles, resulting in growth of CNTs. The as-synthesised CNTs were collected by passing the flow through microporous filters at the downstream of the reactor, while the transparency and sheet resistance was controlled by varying the collection time. The collected CNT networks were transferred to a variety of substrates through the dry press-transfer process. The FC-CVD synthesised and dry deposited CNT networks were of high purity. Furthermore, as the process requires no sonication based dispersion steps the resulting CNT network consisted of exceptionally long CNTs.

Solar Cell Fabrication. The ITO devices were fabricated on a commercially obtained ITO-coated glass substrates (AMG, 9.5 Ω cm^{-2}, 25 × 25 mm^2). The ITO-coated glass substrates were used after sequential cleaning in acetone, isopropanol, and deionized water using an ultrasonic bath (15 min each), followed by drying with nitrogen gas and storing in an oven at 120 °C. Right before use, the ITO-coated glass substrates were subjected to UV-O_3 treatment for 30 min. A 35 nm thick C_{60} layer was densely coated on the ITO glass substrates by using a vacuum thermal evaporator at the constant rate of 0.2 Å/s.

The $MAPbI_3$ perovskite layers were fabricated via Lewis base adduct method described by Ahn *et al*.[5] A 1:1:1 molar ratio mixture of PbI_2 (Alfa Aesar), MAI (Xi'an Polymer Light Technology Corp), and dimethyl sulfoxide (DMSO) (Sigma-Aldrich) was dissolved in

dimethylformamide (DMF) at 50 wt% without heating. The fully dissolved solution was spin coated onto the PEDOT:PSS layer at 3500 rpm for 20 s, with a dropping of 0.3 mL diethyl ether 8s after starting the spin-coating process. The transparent green film, so-called CH_3NH_3I•PbI_2•DMSO adduct film, changed to a dark brown color by heating at 65 °C for 1 min and 100 °C for 4 min.

The prepared CNT films were mechanically transferred to the top of the perovskite layer. A spiro-MeOTAD solution, which was prepared by mixing 72.3 mg of spiro-MeOTAD (Merck), 28.8 µl of 4-*tert*-butyl pyridine and 17.5 µl of lithium bis(trifl uoromethanesulfonyl)imide (Li-TFSI) solution (520 mg Li-TSFI in 1 ml acetonitrile (Sigma–Aldrich, 99.8 %) in 1ml of chlorobenzen, was spin-coated on the CNT film at 1,800 rpm for 30 s. To prepare A PTAA solution, 10 mg of PTAA (EM index, [Mn] = 17,500 g mol-1) was dissolved in 1ml of chlorobenzen with an additive of 4 µl of 4-*tert*-butyl pyridine and 8 µl of lithium bis(trifl uoromethanesulfonyl)imide (Li-TFSI) solution (170 mg Li-TSFI in 1 ml acetonitrile. The PTAA solution was spin-coated at 3,000 rpm for 30 s. In the case of P3HT, 10 mg of P3HT (Sigma-Aldrich) was fully dissolved in 1 ml of chlorobenzene by heating at 70 °C for 1 h. The solution was spin-coated at 3,000 rpm for 30 s.

To prepare encapsulated CNT-P3HT devices, the complete CNT-P3HT devices were covered by a plain glass cover (AMG, 18 × 18 mm^2). Each side of the glass cover were filled with a UV-curable epoxy resin by an automated movable resin dispenser. The encapsulation process was finished by placing the encapsulated devices under a UV treatment for 10 min to harden the epoxy sealant.

Characterizations. Current-voltage (*J–V*) characteristics were measured by software-controlled source meter (Keithley 2400) in dark conditions and 1 sun AM 1.5G simulated sunlight irradiation (100 mW/cm^2) using a solar simulator (Sol 3A Class AAA 64023A,

Oriel), which was calibrated using the KG-5 standard Si-cell. To extract the chemical capacitance, we carried out electrochemical impedance spectroscopy (EIS) analysis with CHI 600D (CH Instruments). Nyquist plots were obtained in the frequency range of 0.05 Hz to 1 MHz under a simulated one-sun illumination with various applied voltages. Each plot was fitted using an equivalent circuit comprised of a series resistance and two resistance-capacitance components.

To evaluate long-term stability of devices, we used a chamber that can maintain constant temperature and illuminate continuously with AM 1.5G one sun condition. The temperature and relative humidity in the chamber were maintained at 20 °C and 15% on average, respectively. Considering average daylight time and actual operation, the light turned continuously on for about 11 hours a day and were off at night time. The encapsulated device was continuously stored in the chamber from 4th November, 2016. Total illumination time was 650 hours.

*Computational calculations***.** Structural optimizations were carried out by using Gaussian09 package at the B3LYP / 6-31G(d) level. Figure S5 shows optimized chemical structures of P3HT pentamer and PTAA trimer.

Conflict of interest

There are no conflicts to declare

Acknowledgments

This work was supported by the Global Frontier R&D Program on Center for Multiscale Energy System funded by the National Research Foundation under the Ministry of Science, ICT & Future Planning, Korea(2012M3A6A7054855),by Grant-in-Aid for Scientific Research (15H05760 and 16H04187), by the CREST project, by the EU-JST funded IRENA

project, and by the Aalto University Energy Efficiency program (AEF) project MOPPI. I.J. thanks the Japan Society for the Promotion of Science for financial support (16F16069). Authors thank Hiroshi Okada for the computational optimization of the polymer configurations in Fig. 3a. The computation was performed by using a super-computer at Research Center for Computational Science, Okazaki, Japan.

Notes and references

1 A. Kojima, K. Teshima, Y. Shirai and T. Miyasaka, *J. Am. Chem. Soc.*, 2009, **131**, 6050–6051.

2 H.-S. Kim, C.-R. Lee, J.-H. Im, K.-B. Lee, T. Moehl, A. Marchioro, S.-J. Moon, R. Humphry-Baker, J.-H. Yum, J. E. Moser, M. Grätzel and N.-G. Park, *Sci. Rep.*, 2012, **2**, 591.

3 M. A. Green, A. Ho-Baillie and H. J. Snaith, *Nat. Photonics*, 2014, **8**, 506–514.

4 J.-H. Im, J. Chung, S.-J. Kim and N.-G. Park, *Nanoscale Res. Lett.*, 2012, **7**, 353.

5 N. Ahn, D.-Y. Son, I.-H. Jang, S. M. Kang, M. Choi and N. Park, *J. Am. Chem. Soc.*, 2015, **137**, 8696–8699.

6 X. Li, D. Bi, C. Yi, J.-D. Decoppet, J. Luo, S. M. Zakeeruddin, A. Hagfeldt and M. Gratzel, *Science*, 2016, **353**, 58–62.

7 W. S. Yang, J. H. Noh, N. J. Jeon, Y. C. Kim, S. Ryu, J. Seo and S. I. Seok, *Science*, 2015, **348**, 1234-1237..

8 J. H. Noh, S. H. Im, J. H. Heo, T. N. Mandal and S. Il Seok, *Nano Lett.*, 2013, **13**, 1764–1769.

9 Y. Yang, J. Xiao, H. Wei, L. Zhu, D. Li, Y. Luo, H. Wu and Q. Meng, *RSC Adv.*, 2014, **4**, 52825–52830.

10 W. A. Laban and L. Etgar, *Energy Environ. Sci.*, 2013, **6**, 3249–3253.

11 L. Etgar, P. Gao, Z. Xue, Q. Peng, A. K. Chandiran, B. Liu, M. K. Nazeeruddin and M. Grätzel, *J. Am. Chem. Soc.*, 2012, **134**, 17396–17399.

12 J. Liu, Y. Wu, C. Qin, X. Yang, T. Yasuda, A. Islam, K. Zhang, W. Peng, W. Chen and L. Han, *Energy Environ. Sci.*, 2014, **7**, 2963–2967.

13 A. Mei, X. Li, L. Liu, Z. Ku, T. Liu, Y. Rong, M. Xu, M. Hu, J. Chen, Y. Yang, M. Gratzel and H. Han, *Science*, 2014, **345**, 295–298.

14 J. You, L. Meng, T.-B. Song, T.-F. Guo, Y. (Michael) Yang, W.-H. Chang, Z. Hong, H. Chen, H. Zhou, Q. Chen, Y. Liu, N. De Marco and Y. Yang, *Nat. Nanotechnol.*, 2015, **11**, 75–81.

15 Z. Li, S. A. Kulkarni, P. P. Boix, E. Shi, A. Cao, K. Fu, S. K. Batabyal, J. Zhang, Q. Xiong, L. H. Wong, N. Mathews and S. G. Mhaisalkar, *ACS Nano*, 2014, **8**, 6797–6804.

16 K. Aitola, K. Sveinbjörnsson, J.-P. Correa-Baena, A. Kaskela, A. Abate, Y. Tian, E. M. J. Johansson, M. Grätzel, E. I. Kauppinen, A. Hagfeldt and G. Boschloo, *Energy Environ. Sci.*, 2016, **9**, 461–466.

17 S. Information, S. N. Habisreutinger, T. Leijtens, G. E. Eperon, S. D. Stranks, R. J. Nicholas and H. J. Snaith, *Nano Lett.*, 2014, **14**, 5561–5568.

18 F. Wang, M. Endo, S. Mouri, Y. Miyauchi, Y. Ohno, A. Wakamiya, Y. Murata, K. Matsuda and A. Manuscript, *Nanoscale*, 2016, **8**, 11882–11888.

19 E. L. Unger, E. T. Hoke, C. D. Bailie, W. H. Nguyen, A. R. Bowring, T. Heumüller, M. G. Christoforo and M. D. McGehee, *Energy Environ. Sci.*, 2014, **7**, 3690–3698.

20 H. Sung, N. Ahn, M. S. Jang, J. Lee, H. Yoon, N. Park and M. Choi, *Adv. Energy Mater.*, 2016, **6**, 1501873.

21 J. Yoon, H. Sung, G. Lee, W. Cho, N. Ahn, H. S. Jung and M. Choi, *Energy Environ. Sci.*, 2017, **10**, 337–345.

22 H. Yoon, S. M. Kang, J.-K. Lee and M. Choi, *Energy Environ. Sci.*, 2016, **9**, 2262–2266.

23 N. Ahn, K. Kwak, M. S. Jang, H. Yoon, B. Y. Lee, J. Lee, P. V Pikhitsa, J. Byun and M. Choi, *Nat. Commun.*, 2016, **7**, 13422.

24 M. M. Lee, J. Teuscher, T. Miyasaka, T. N. Murakami and H. J. Snaith, *Science*, 2012, **338**, 643–647.

25 J. Burschka, N. Pellet, S.-J. Moon, R. Humphry-Baker, P. Gao, M. K. Nazeeruddin and M. Grätzel, *Nature*, 2013, **499**, 316–319.

26 M. Liu, M. B. Johnston and H. J. Snaith, *Nature*, 2013, **501**, 395–398.

27 N. J. Jeon, J. H. Noh, Y. C. Kim, W. S. Yang, S. Ryu and S. Il Seok, *Nat. Mater.*, 2014, **13**, 897–903.

28 B. Conings, L. Baeten, C. De Dobbelaere, J. D'Haen, J. Manca and H.-G. Boyen, *Adv. Mater.*, 2014, **26**, 2041–2046.

29 Y. Guo, C. Liu, K. Inoue, K. Harano, H. Tanaka and E. Nakamura, *J. Mater. Chem. A*, 2014, **2**, 13827–13830.

30 A. Kaskela, A. G. Nasibulin, M. Y. Timmermans, B. Aitchison, A. Papadimitratos, Y. Tian, Z. Zhu, H. Jiang, D. P. Brown, A. Zakhidov and E. I. Kauppinen, *Nano Lett*. 2010, **10**, 4349.

31 A. G. Nasibulin, A. Kaskela, K. Mustonen, A. S. Anisimov, V. Ruiz, S. Kivistö, S. Rackauskas, M. Y. Timmermans, M. Pudas, B. Aitchison, M. Kauppinen, D. P. Brown, O. G. Okhotnikov, and E. I. Kauppinen, *ACS Nano* 2011, **5**, 3214.

32 W. J. Lee, E. Ramasamy, D. Y. Lee, J. S. Song, *ACS Appl. Mater. Interfaces* 2009, **1**, 1145.

33 M. Gong, T. A. Shastry, Y. Xie, M. Bernardi, D. Jasion, K. A. Luck, T. J. Marks, J. C. Grossman, S. Ren, M. C. Hersam, *Nano Lett.* 2014, **14,** 5308.

34 H. W. Lee, Y. Yoon, S. Park, J. H. Oh, S. Hong, L. S. Liyanage, H. Wang, S. Morishita, N. Patil, Y. J. Park, J. J. Park, A. Spakowitz, G. Galli, F. Gygi, P. H.-S. Wong, J. B.-H. Tok, J. M. Kim, Z. Bao, *Nat. Commun.* 2011, **2**, 541.

35 T. Schuettfort, H. J. Snaith, A. Nish, R. J. Nicholas, *Nanotechnology* 2010, **21**, 25201.

36 M. J. Frisch, G. W. Trucks, H. B. Schlegel, G. E. Scuseria, M. A. Robb, J. R. Cheeseman, G. Scalmani, V. Barone, B. Mennucci, G. A. Petersson, H. Nakatsuji, M. Caricato, X. Li, H. P. Hratchian, A. F. Izmaylov, J. Bloino, G. Zheng, J. L. Sonnenberg, M. Hada, M. Ehara, K. Toyota, R. Fukuda, J. Hasegawa, M. Ishida, T. Nakajima, Y. Honda, O. Kitao, H. Nakai, T. Vreven, J. A. Montgomery Jr., J. E. Peralta, F. Ogliaro, M. Bearpark, J. J. Heyd, E. Brothers, K. N. Kudin, V. N. Staroverov, R. Kobayashi, J. Normand, K. Raghavachari, A. Rendell, J. C. Burant, S. S. Iyengar, J. Tomasi, M. Cossi, N. Rega, J. M. Millam, M. Klene, J. E. Knox, J. B. Cross, V. Bakken, C. Adamo, J. Jaramillo, R. Gomperts, R. E. Stratmann, O. Yazyev, A. J. Austin, R. Cammi, C. Pomelli, J. W. Ochterski, R. L. Martin, K. Morokuma, V. G. Zakrzewski, G. A. Voth, P. Salvador, J. J. Dannenberg, S. Dapprich, A. D. Daniels, Ö. Farkas, J. B. Foresman, J. V Ortiz, J. Cioslowski, D. J. Fox, *Gaussian Inc.* 2009, Wallingford CT.

37 G. Li, R. Zhu, Y. Yang, *Nat. Photonics* 2012, **6**, 153.

38 S. Holliday, R. S. Ashraf, A. Wadsworth, D. Baran, S. A. Yousaf, C. B. Nielsen, C.-H. Tan, S. D. Dimitrov, Z. Shang, N. Gasparini, M. Alamoudi, F. Laquai, C. J. Brabec, A. Salleo, J. R. Durrant, I. McCulloch, *Nat. Commun.* 2016, **7**, 11585.

39 D. R. Barbero, S. D. Stranks, *Adv. Mater.* 2016, **28,** 9668.

40 D. Tuncel, *Nanoscale* 2011, **3**, 3545.

41 A. Dualeh, T. Moehl, M. K. Nazeeruddin, M. Grätzel, *ACS Nano* 2013, **7**, 2292.

42 A. Abate, D. J. Hollman, J. Teuscher, S. Pathak, R. Avolio, G. D'Errico, G. Vitiello, S. Fantacci, H. J. Snaith, *J. Am. Chem. Soc.* 2013, **135**, 13538.

43 J. Burschka, A. Dualeh, F. Kessler, E. Baranoff, N.-L. Cevey-Ha, C. Yi, M. K. Nazeeruddin, M. Grätzel, *J. Am. Chem. Soc.* 2011, **133**, 18042.

44 A. Abate, T. Leijtens, S. Pathak, J. Teuscher, R. Avolio, M. E. Errico, J. Kirkpatrik, J. M. Ball, P. Docampo, I. McPherson, H. J. Snaith, *Phys. Chem. Chem. Phys.* 2013, **15**, 2572.

45 W. Chen, Y. Wu, Y. Yue, J. Liu, W. Zhang, X. Yang, H. Chen, E. Bi, I. Ashraful, M. Grätzel, L. Han, *Science* 2015, **350**, 944

46 X. Li, M. Ibrahim Dar, C. Yi, J. Luo, M. Tschumi, S. M. Zakeeruddin, M. K. Nazeeruddin, H. Han, M. Grätzel, *Nat. Chem.* 2015, **7**, 703

47 H. Tsai, W. Nie, J.-C. Blancon, C. C. Stoumpos, R. Asadpour, B. Harutyunyan, A. J. Neukirch, R. Verduzco, J. J. Crochet, S. Tretiak, L. Pedesseau, J. Even, M. A. Alam, G. Gupta, J. Lou, P. M. Ajayan, M. J. Bedzyk, M. G. Kanatzidis, A. D. Mohite, *Nature* 2016, **536**, 312

48 Z. Wang, D. P. McMeekin, N. Sakai, S. van Reenen, K. Wojciechowski, J. B. Patel, M. B. Johnston, H. J. Snaith, *Advanced Materials* 2017, **29**, 1604186

49 S. S. Shin, E. J. Yeom, W. S. Yang, S. Hur, M. G. Kim, J. Im, J. Seo, J. H. Noh, S. I. Seok, *Science* 2017, **356**, 167

50 J. You, L. Meng, T.-B. Song, T.-F. Guo, Y. Yang, W.-H. Chang, Z. Hong, H. Chen, H. Zhou, Q. Chen, Y. Liu, N. De Marco, Y. Yang, *Nat. Nano.* 2016, **11**, 75.

51 T. Leijtens, G. E. Eperon, S. Pathak, A. Abate, M. M. Lee, H. J. Snaith, *Nat. Commun.* 2013, **4**, 1.

52 T. Leijtens, J. Lim, J. Teuscher, T. Park, H. J. Snaith, *Adv. Mater.* 2013, **25**, 3227.

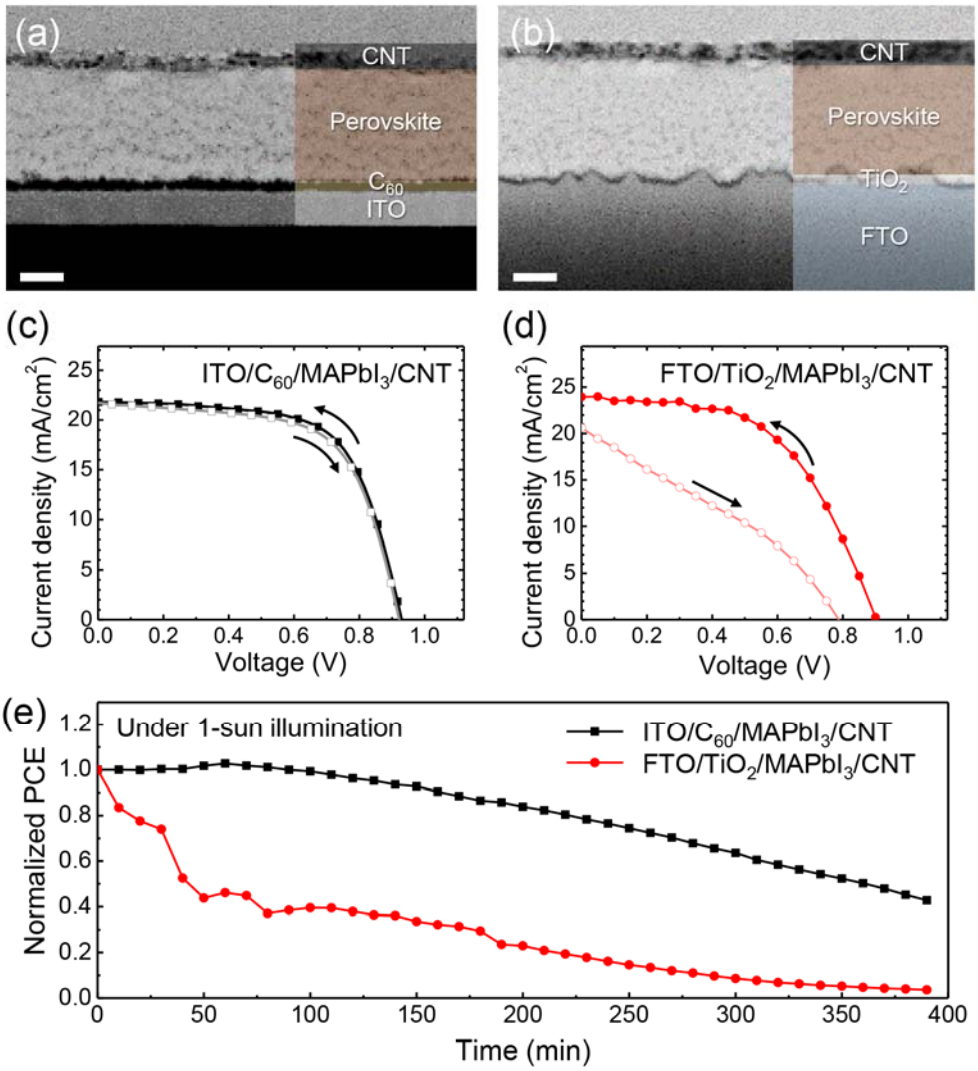

Fig. 1 Cross-sectional SEM images of (a) ITO/C_{60}/$MAPbI_3$/CNT device and (b) FTO/TiO_2/$MAPbI_3$/CNT. The forward and backward $J-V$ curves of (c) the C_{60}-based device and (d) the TiO_2-based device, respectively. (e) Time evolution of normalized PCEs of C_{60}- and TiO_2- based devices without encapsulation

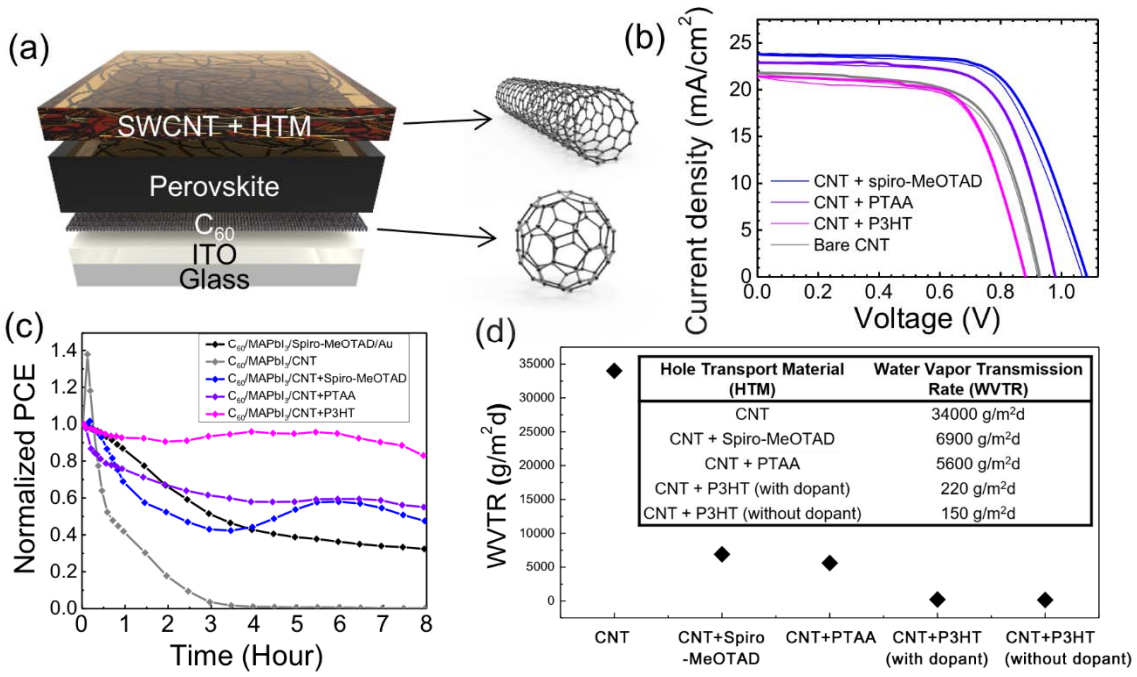

Hole Transport Material (HTM)	Water Vapor Transmission Rate (WVTR)
CNT	34000 g/m²d
CNT + Spiro-MeOTAD	6900 g/m²d
CNT + PTAA	5600 g/m²d
CNT + P3HT (with dopant)	220 g/m²d
CNT + P3HT (without dopant)	150 g/m²d

Fig. 2 (a) Graphical illustration of carbon allotropes sandwich approach used in this work (glass/ITO/C_{60}/ $MAPbI_3$/HTM/CNT). Perovskite active layer is sandwiched by fullerenes and carbon nanotubes entangled with a hole-transporting material. (b) Reverse (thick) and forward (thin) bias *J*–*V* curves of the devices used in this work, namely CNT, CNT with spiro-MeOTAD, CNT with PTAA, or CNT with P3HT as the top electrode under one sun (AM1.5G illumination, 100 mW cm^{-2}). (c) Light-induced charge stability test of unencapsulated devices with CNT, CNT with spiro-MeOTAD, CNT with PTAA, CNT or P3HT as the top electrode, and also of the reference device with spiro-MeOTAD wth Au as the top electrode**.** (d) WVTR figure of merit with a raw data as an inset.

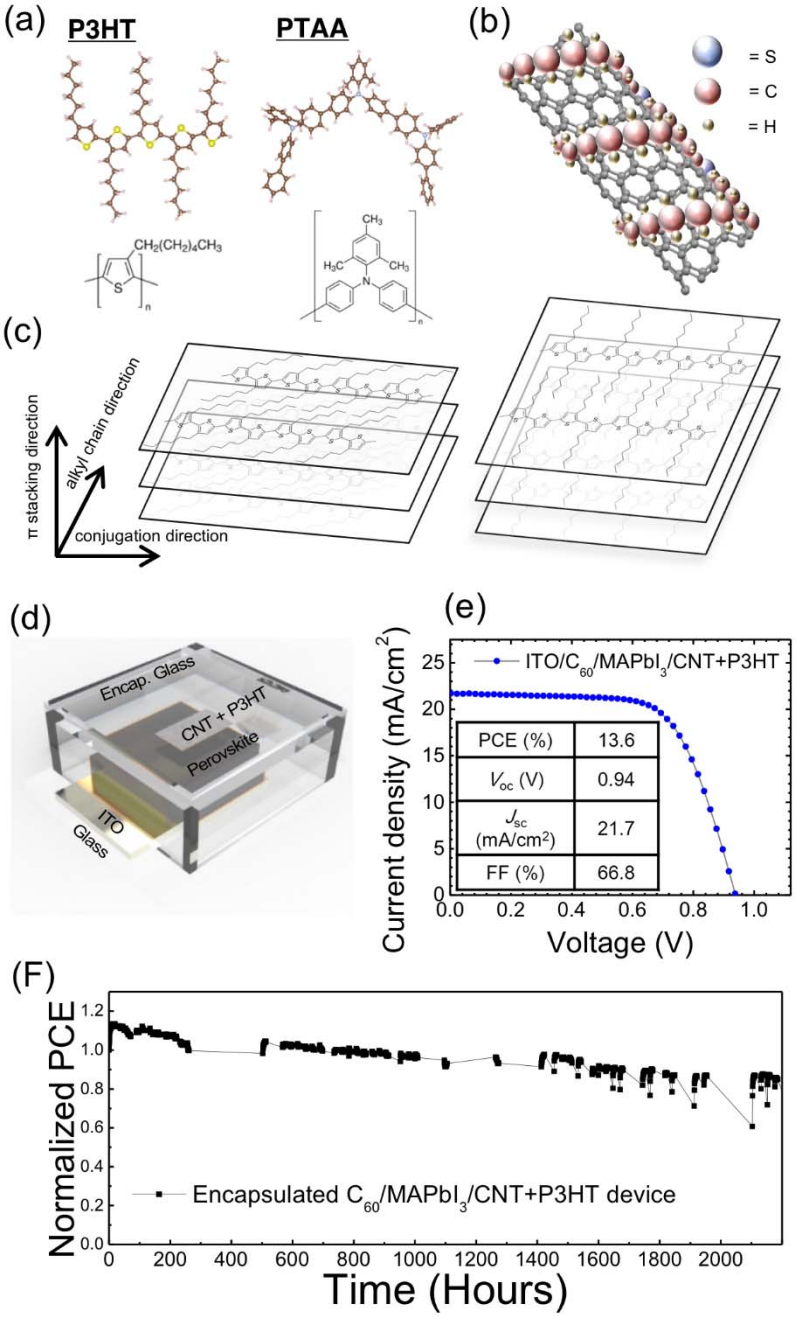

Fig. 3 (a) Optimized configuration of P3HT pentamer (left) and PTAA trimer (right). The computational studies were carried out by using Gaussian09 and details were described in experimental section and Figure. S5. (b) Exemplary P3HT packing arrangements characterized by different amount of interdigitation of the alkyl side chains. Comb-like arrangement (left) and fishbone-like arrangement (right). (c) Graphical Illustration of P3HT interacting with a CNT. (d),(e) Graphical illustration and the $J-V$ curve of the best CNT+P3HT-based device which we encapsulated using glass, and the corresponding photovoltaic table as an inset. (f) Light-induced stability in ambience test of the glass-encapsulated CNT+P3HT-based device.

Electrode type	Scan direction	V_{OC} (V)	J_{SC} (mA/cm^2)	FF	PCE (%)	Hysteresis Index
C_{60}/$MAPbI_3$/Bare CNT	Reverse	0.93	21.8	0.65	13.2	0.038
	Forward	0.92	21.8	0.63	12.7	
TiO_2/$MAPbI_3$/Bare CNT	Reverse	0.90	23.9	0.54	11.6	0.553
	Forward	0.79	20.6	0.32	5.18	

Table 1. Photovoltaic data of the CNT-based PSCs with C_{60} and TiO_2 as the electron-transporting layer under one sun (AM1.5G illumination, 100 mW cm^{-2}) and their hysteresis indices.

Electrode type		V_{oc} (V)	J_{sc} (mA/cm^2)	FF	PCE (%)	Cost
Bare CNT	Average	0.93 ± 0.00	21.2 ± 1.7	0.63 ± 0.03	12.4 ± 0.9	<3.6%
	Best	0.93	21.8	65.0	13.2	
CNT + spiro-MeOTAD	Average	1.05 ± 0.03	22.8 ± 0.9	0.66 ± 0.02	16.0 ± 0.4	<13.5%
	Best	1.08	23.8	66.1	17.0	
CNT + PTAA	Average	0.99 ± 0.01	23.3 ± 0.5	0.65 ± 0.02	14.9 ± 0.4	<6.0%
	Best	0.98	23.0	67.7	15.30	
CNT + P3HT	Average	0.91 ± 0.05	21.1 ± 0.4	0.61 ± 0.04	11.7 ± 1.1	<5.5%
	Best	0.94	21.7	66.8	13.6	

Table 2 Average and best photovoltaic data of the solar cell devices with different cathode types under one sun (AM1.5G illumination, 100 mW cm^{-2}) and their estimated fabrication costs relative to conventional PSCs (FTO/TiO_2/mesoporous-TiO_2/$MAPbI_3$/spiro-MeOTAD/Au).

Carbon-Sandwiched Perovskite Solar Cell